13th International Symposium on Turbulence and Shear Flow Phenomena (TSFP13)
Montreal, Canada, June 25–28, 2024

REDUCED ORDER MODEL BASED INVESTIGATIONS INTO THE DRAG REDUCTION BREAKDOWN IN FLOW OVER BLADE RIBLETS

Bianca Viggiano
Department of Mechanical Engineering
Polytechnique Montréal
2500 Chem. de Polytechnique
Montréal, Quebec, H3T 1J4, CA
bianca.viggiano@polymtl.ca

Benjamin Minnick
Submarine Maneuvering and Control Division
Naval Surface Warfare Center Carderock Division
9500 MacArthur Blvd
West Bethesda, Maryland, 20817, USA
benjamin.a.minnick.civ@us.navy.mil

Xiaowei Zhu
Department of Mechanical Engineering
Portland State University
1930 SW 4th Ave
Portland, Oregon 97201, USA
xz3@pdx.edu

Dennice F. Gayme
Department of Mechanical Engineering
Johns Hopkins University
3400 N Charles St
Baltimore, Maryland 21218, USA
dennice@jhu.edu

ABSTRACT

The restricted nonlinear (RNL) model is employed as low-order representation of turbulent flow over blade riblets at $Re_\tau = 395$. The ability of the model to capture the salient features of these flows is first assessed in terms of the first and second-order statistics, which are used to verify that drag reduction and the onset of drag increase are well described by the RNL model. The roughness function is then decomposed and the RNL simulations are shown to reproduce the overall trends of the function and its constituent parts over a range of riblet spacings. Spectra of Reynolds shear stress demonstrates that the stresses known to be associated with the Kelvin-Helmholtz (KH)-like rollers, that have been tied the break-down of riblet induced drag-reduction and onset drag-increases at higher spacings, are captured through the limited streamwise scales in the RNL model. The curves arising through integration of the stresses over the spanwise and streamwise wavenumbers associated with KH structures further demonstrate that the RNL model reproduces general trends over the wall-normal extent. However, the overall added stresses due to the presence of riblets, as well as the contributions from the KH-like rollers are over-predicted by the RNL model. These results indicate that nonlinear interactions not captured in the current model may play a role in the underlying phenomena, which motivates future study using a higher-order RNL representation.

INTRODUCTION

Skin-friction drag is a significant contributor to transport efficiency loss in a range of applications (Bushnell, 1983; Viswanath, 2002; Spalart & McLean, 2011). An approach that has shown success in reducing this drag is the addition of two dimensional micro-scale surface protrusions, in the form of “riblets” (García-Mayoral & Jiménez, 2011*a*). At low Reynolds numbers riblets can provide up to a $\sim$10% decrease in drag compared to the same flow over a smooth wall (García-Mayoral & Jiménez, 2011*a*; Walsh, 1982; Bechert *et al.*, 1997). However, the specific nature of the changes in skin-friction drag depend on the riblet geometry, spacing, and flow properties. One parameter that has proven useful in characterizing the skin-friction drag over the riblets is the characteristic length of the micro-grooves, which is defined as the square root of the cross-sectional area of a groove $\ell_g^+ = (A_g^+)^{1/2}$ (Walsh, 1980; Luchini *et al.*, 1991; García-Mayoral & Jiménez, 2011*a*). Here, the superscript $+$ refers to scaling by the friction velocity, u_τ, and kinematic viscosity, ν. It is well established that common measures of drag (e.g. the roughness function, slip length) adhere to a fairly ‘universal’ collapse with ℓ_g^+, following a linear relationship in the viscous regime up to the minimum drag level at $\ell_g^+ \approx 11$, see Bechert *et al.* (1997) and Luchini *et al.* (1991); Luchini (1996) for details. Then, as the riblet spacing continues to increase, the skin-friction drag begins to increase until it surpasses that seen in flow over a smooth wall (Jiménez, 2004). The physics behind drag alteration by riblets has been studied in great detail, but there is still much disagreement of the mechanisms driving the onset of drag increase (Goldstein & Tuan, 1998; Choi *et al.*, 1993; García-Mayoral & Jiménez, 2011*a*; Modesti *et al.*, 2021). Successful design and installation of riblets in practical applications requires further understanding of the factors that contribute to this so-called breakdown of riblet-induced drag reduction.

Skin-friction drag changes due to surface modification are often quantified in terms of the roughness function, $\Delta U^+ \equiv U_S^+ - U_R^+$, which evaluates the shift of the mean streamwise velocity profiles of a rough and smooth wall (respectively U_R^+ and U_S^+) in the log region. The roughness function gives a first order quantification of the riblet imposed drag reduction or increase on the flow. The mechansims underlying these changes can be investigated in more detail by decomposing ΔU^+. For example, García-Mayoral & Jiménez (2011*b*) used this approach to study the slip velocity, as well as the extra Reynolds stress contributions to the breakdown of drag reduction over blade riblets. That work indicated that Kelvin-Helmholtz (KH) rollers appear at riblet spacings at which skin-friction drag begins to rise, and suggested that a KH instability may play a role in the breakdown. However, further investigations into the roughness function over a range of geometries carried out by Endrikat *et al.* (2021*a*) demonstrated that while the onset of KH rollers contributes to the roughness function for certain geometries, they are not present in other geometries even when similar drag increases are observed. These studies demonstrate the need for further study to fully characterize the mechanisms underlying the breakdown of riblet induced drag reduction.

Developing the required understanding is challenging due to the difficulties posed by both experimental and numerical studies of flow over these micro-structures. The required resolution near the riblet tips in a high-fidelity direct numerical simulation (DNS) can result in a tenfold increase in computational expense over a smooth wall simulation at the same Reynolds number. These computational challenges have led researchers to pursue more computationally tractable approaches such as minimal channel simulations (Chung *et al.*, 2015; Endrikat *et al.*, 2021*b*), or analytical approaches such as resolvent analysis (Chavarin & Luhar, 2020). While both of these methods have proven useful in the study of riblet-induced drag reduction and its breakdown, further questions remain.

Here we employ restricted nonlinear (RNL) simulations to study flow over riblets as an alternative approach. The RNL framework has the benefit of computational tractability, as well as a means to directly probe the impact of particular flow scales through the model parametrization, as discussed in e.g., Thomas *et al.* (2015); Gayme & Minnick (2019); Minnick & Gayme (2019); Minnick (2022). More specifically, the RNL dynamics comprise a streamwise constant mean flow coupled to a highly restricted streamwise varying perturbation field that is linear in the perturbations (Farrell & Ioannou, 2012; Thomas *et al.*, 2014). The model is parameterized by prescribing the streamwise varying scales supporting the perturbation field. These modeled streamwise scales are typically chosen to coincide with those maximizing dissipation in the outer-layer. This parameterization is chosen because it leads to accurate reproduction of the low-order statistics and spectral features of turbulent smooth-wall channel flows at low to moderate Reynolds numbers (Bretheim *et al.*, 2015; Gayme & Minnick, 2019; Minnick & Gayme, 2019). The dynamical restriction of the perturbation allows flow field realizations at highly reduced computational costs in comparison to DNS. The success of the model in reproducing cross-stream interactions suggests its utility in the study of flow over riblets, where secondary motions in the cross-stream are known to be important (Goldstein & Tuan, 1998).

The study herein is based on RNL simulations of flow over blade geometries for a range of spacings that capture behavior both before maximum riblet induced skin-friction drag reduction (i.e., $\leq \ell_g^+ = 11$) and as the surface transitions to drag-increasing. The main analysis focuses on decomposition of the roughness function to assess both ability of the RNL model to predict the different mechanisms that have been previously studied and to directly probe the role of streamwise flow scales corresponding to KH rollers. The later study is facilitated by the fact the the modes associated with the typical RNL model parametrization coincide with those known to contribute to the onset of the Kelvin-Helmholtz instability. The notion of isolating of the affect of the KH rollers is motivated in part by the success of resolvant analysis based studies which were able to accurately predict drag reduction and the associated breakdown from KH rollers based on isolation of the prescribed modes (Chavarin & Luhar, 2020). The results herein first demonstrate that the RNL simulations reproduce key features of the flow over blade riblets for a range of characteristic lengths. The simplified RNL dynamics are then used to isolate the role of the limited active streamwise modes the drag alteration. Further analysis based on a decomposition of the roughness function and the added stresses is employed to understand the extent to which the RNL representation can capture the KH rollers observed in Endrikat *et al.* (2021*a*); García-Mayoral & Jiménez (2011*a*).

The remainder of this paper is organized as follows. The next section we describe the RNL model, riblet configurations and simulation set up for this study. The results section then reports the low-order statistics obtained in the RNL simulations followed by a more detailed analysis of the components comprising the roughness function. Finally we conclude the paper and discuss directions for further study.

RNL MODEL AND NUMERICAL METHOD

The RNL governing equations are formed by decomposing the total velocity and pressure fields into the streamwise averaged mean and perturbations (about that mean). Specifically, the total velocity $\mathbf{u}_T = \mathbf{U} + \mathbf{u}$, where the mean velocity is defined as $\mathbf{U}(y,z,t) = \langle \mathbf{u}_T \rangle_x$, with the angle brackets indicating streamwise averaging, and $\mathbf{u}(x,y,z,t)$ denoting the perturbations. The decomposition and filtering is applied to the pressure field in an analogous manner.

The riblets along the wall are applied using the immersed boundary method of Peskin (2002). In particular, through the application of a force, $\mathbf{f}$, that is defined to enforce zero velocity within the riblets at each time step. This force is set to zero outside of the riblets. The resulting forced RNL mean, perturbation and continuity equations are given by:

$$\partial_t \mathbf{U} + \mathbf{U}\cdot\nabla\mathbf{U} + \langle \mathbf{u}\cdot\nabla\mathbf{u}\rangle_x + \nabla P/\rho - \nu\nabla^2\mathbf{U} = \langle \mathbf{f}\rangle_x \quad (1)$$

$$\partial_t \mathbf{u} + \mathbf{U}\cdot\nabla\mathbf{u} + \mathbf{u}\cdot\nabla\mathbf{U} + \nabla p/\rho - \nu\nabla^2\mathbf{u} = (\mathbf{f} - \langle \mathbf{f}\rangle_x) \quad (2)$$

$$\nabla\cdot\mathbf{U} = \nabla\cdot\mathbf{u} = 0 \quad (3)$$

where ρ and ν are, respectively, the fluid density and kinematic viscosity, ∇ is the gradient operator and ∇^2 is the Laplacian operator.

The riblet simulations are carried out in a half-channel configuration using the pseudo-spectral code (JHU-LESGO, 2019). This code employs spectral derivatives in the streamwise and spanwise directions with the 3/2 rule for dealiasing. In the wall-normal direction, a second-order finite differencing scheme with a hyperbolic-tangent stretched coordinate system (Vinokur, 1983; Jelly *et al.*, 2014) is used. The second-order Adams-Bashforth method is used for time stepping. Periodic boundary conditions are employed in the streamwise and spanwise directions. Riblets are imposed on the bottom wall as described above, and a stress-free boundary condition is imposed at the top of the domain.

Table 1 describes the blade riblet geometry and details the different parameters for the four riblet spacings, s^+, that are considered herein. In all configurations, the cross-sectional area of the rough wall flow matches that of the smooth wall flow, and we define our half-channel height, δ, from the mean height of the riblets to the top of the domain. The friction Reynolds number for each case is set to $\mathrm{Re}_\tau = 395$ and is defined as $\mathrm{Re}_\tau = u_\tau\delta/\nu$, where u_τ is the friction velocity. The streamwise wavenumbers supporting the perturbation dynamics are $k_x\delta = 15.5, 16, 16.5$. The corresponding wavelengths are coincident with the outer-layer peak in the dissipation spectra. This model parametrization has been shown to produce

Table 1. Characteristics of blade geometries considered, including the spacing s^+, height h^+, corresponding groove size ℓ_g^+, and the thichness to spacing ratio, $b/s = 1/5$.

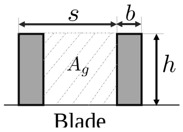

Case	s^+	h^+	ℓ_g^+	b/s
BL10	10	5	6.33	1/5
BL20	20	10	12.65	1/5
BL30	30	15	18.97	1/5
BL40	40	20	25.30	1/5

accurate results in smooth wall flows at similar Reynolds numbers, see e.g. Gayme & Minnick (2019).

Although the specified friction Reynolds number $Re_\tau = 395$ is defined with respect to the mean height of the riblets, we must redefine our coordinates system after the simulation is completed in order to accurately compare the flow over the smooth and riblet lined walls. For this we employ the concept of the origin of turbulence introduced by Luchini (1996). In particular, the origin of turbulence is used to provide a reference 'smooth wall' for the riblets where near-wall turbulent eddies are perceived to originate. In practice, we define this virtual origin, denoted ℓ_T^+, by first calculating the largest slope of the Reynolds stress profile of the rough wall flow for the drag optimal case ($\ell_g^+ = 12.65$ in our simulations) and then finding the height associated with that value in the flow over the smooth wall. The virtual origin for all remaining riblet spacings is then computed based on maintaining a constant ratio of ℓ_T^+/h^+.

RESULTS

The mean streamwise velocity profiles for each of the four considered cases are shown in figure 1(a), with the smooth wall profile included as a dashed line for comparison. To simplify the notation in the figures and throughout this section we abuse the notation by denoting the steamwise, spanwise and temporally averaged streamwise velocity component in viscous units as U^+, i.e. $U^+ := \langle \overline{U}^+ \rangle_z = \langle \overline{u_T}^+ \rangle_{xz}$, where the overbar denotes time-averaging. Herein, the wall-normal direction is set such that $y^+ = 0$ at the origin of turbulence (i.e., ℓ_T^+ below the riblet tip). The profiles in figure 1(a) provide an initial indication of the ability of the RNL model to accurately model the first-order statistics of flow over the blade riblets. Using the smooth wall as a reference, it is immediately evident in figure 1(a) that the two smallest groove sizes, $\ell_g^+ \approx 6$ and 13, increase the fluid momentum while the largest two riblet spacings, $\ell_g^+ \approx 19$ and 25, decrease the momentum of the fluid. These trends are even more clear in figure 1(b), which depicts the difference between the smooth and rough wall velocity profiles for each case.

Figure 2(a) presents the Reynolds shear stress as a function of wall normal location. We note that the two drag reducing riblet spacings, $\ell_g^+ \approx 6$ and 13, follow the profile of the smooth wall closely. However, as the spacing increases, $\ell_g^+ \geq 19$, deviations arise because this flow is no longer similar enough to smooth walls for the shift based on the virtual origin to fully capture the near-wall effects (Garcia-Mayoral *et al.*, 2019). These results reflect the same trends observed in Endrikat *et al.* (2021*a*) for blade riblets with similar spacings.

We next investigate the ability of the RNL framework to capture different mechanisms that are known to contribute to the roughness function ΔU^+. Following the work of Endrikat *et al.* (2021*a*), the mean streamwise velocity shift induced by the rough surface (from the smooth wall velocity profile), at a height in the log-law region y_c^+, can be decomposed as

$$\Delta U^+(y_c^+) = U_s^+ - U^+ = \Delta U_t^+ + \Delta U_{uv}^+, \tag{4}$$

where

$$\Delta U_t^+ = U_s^+(y_t^+) - U^+(y_t^+) \tag{5}$$

$$\Delta U_{uv}^+ = \int_{y_t^+}^{y_c^+} \frac{\delta_s^+ - y^+}{\delta_s^+} - \frac{\delta'^+ - y^+}{\delta^+} \mathrm{d}y^+ + \int_{y_t^+}^{y_c^+} \overline{u'v'}_s^+ - \overline{u'v'}^+ - \overline{\tilde{u}\tilde{v}}^+ \mathrm{d}y^+ \tag{6}$$

Here ΔU_t^+ is the difference in the mean velocity between the smooth and rough wall at the top of the riblet, y_t^+, and U_s^+ is the velocity of the smooth wall. The added stress contribution, ΔU_{uv}^+ is the difference between the integrated stresses (from the riblet top to some specified location y_c^+) obtained from the smooth and rough walls simulations. Here δ_s^+ is the smooth wall Reynolds number, δ^+ is the rough wall Reynolds number based on the initialization of the simulation (i.e., we set $\delta^+ = 395$ based on the mean riblet height origin), and δ'^+ is the adjusted Reynolds number based on the adjusted origin of turbulence, ℓ_T^+. In this formulation, the added stresses ΔU_{uv}^+ can be considered a measure of the mismatch of the Reynolds numbers due to both the riblets and the use of the virtual origin as the lower integration bound for both the smooth and rough wall cases (Endrikat *et al.*, 2021*a*).

Figure 2(b) shows the different terms in the decomposition of the roughness function described in Eqn. (4), including the added stresses (▷), the mean velocity difference at the riblet tip location y_t^+ (○), $\Delta U^+(y_c^+)$ computed using the sum in (4) (□) and ΔU^+ computed based on the average velocity difference in the log region ($50 < y^+ < 10$) (- -). We also include the $U_s^+ - U^+$ profile from the minimal channel data in Modesti *et al.* (2019) (◆). These results show that the RNL data closely follows known trends for the drag reducing cases. The roughness function, computed from both the decomposition, $\Delta U_t + \Delta U_{uv}$, and the log region comparison, $U^+ - U_s^+$, show negative values, indicating an increase in momentum transport in the flow over the riblets in comparison to that over the smooth wall. In addition, the added stresses show minimal contributions for $\ell_g^+ < 15$. For the two drag increasing cases, spacings of $s^+ = 30$ and 40 (corresponding to $\ell_g^+ = 19$ and 25.3), the overall trends of the RNL model and the minimal channel profiles are consistent although the RNL model overpredicts the drag increase for the two larger spacings versus the minimal channel blade riblet results. This difference is less pronounced in the ΔU^+ obtained based on the velocity curves versus the calculation from the terms in Eqn. (4). Given the previous work indicating the presence of Kelvin-Holmholtz for the drag increasing spacings (García-Mayoral & Jiménez, 2011*a*; Endrikat *et al.*, 2021*a*), we next further investigate the discrepancies by examining the Kelvin-Holmholtz-like contributions to the added stresses.

Kelvin-Helmholtz structures have been associated with particular spanwise and streamwise wavenumbers (García-Mayoral & Jiménez, 2011*b*), thus the first step in our analysis is verifying that the RNL simulations reproduce the associated high levels of Reynolds stress over these wave number ranges. Figure 3 presents the premultiplied 2D co-spectra of

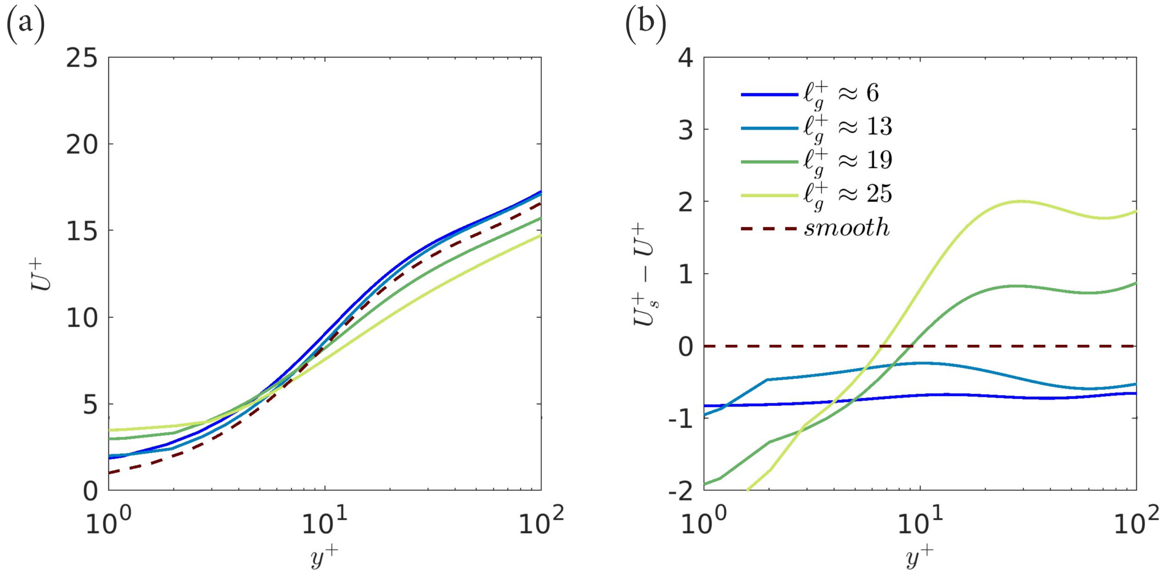

Figure 1. Profiles of the spatially (streamwise and spanwise) and time-averaged streamwise velocity U^+ (a) and the momentum difference between smooth and rough wall flow $U^+_{smooth} - U^+$ (b) as a function of y^+, where $y^+ = 0$ is at the virtual origin.

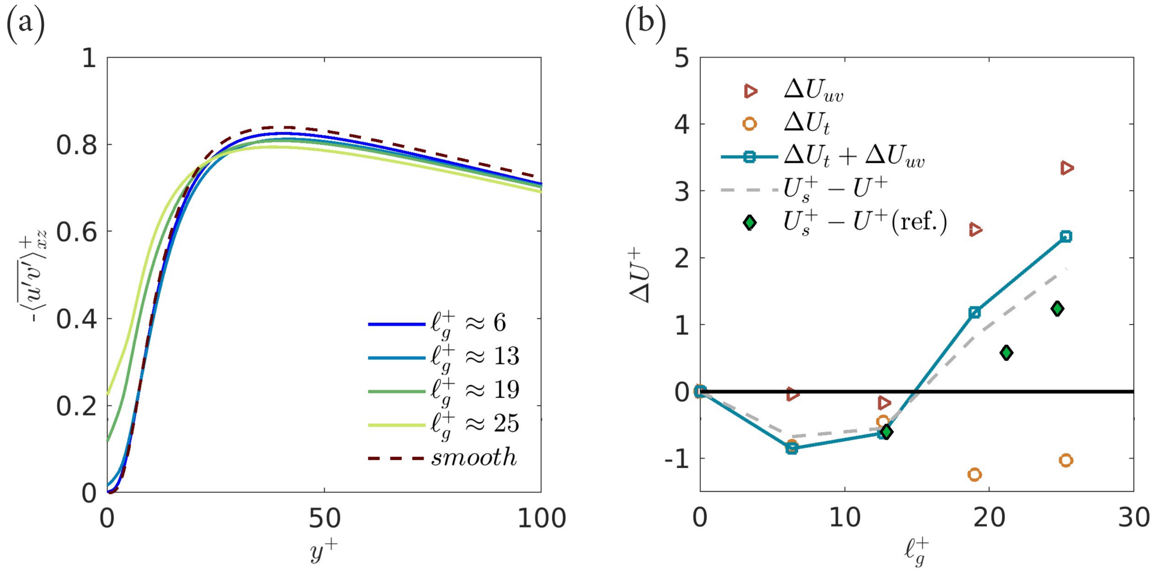

Figure 2. The spatially and temporally averaged and Reynolds shear stress -$\langle\overline{u'v'}\rangle_{xz}$ (a), as a function of the wall normal position y^+ and the contributions of drag (b), as presented in Eqn. (4). Specifically, ΔU^+, is decomposed into the added stress (▷) and riblet tip speed difference (○) are provided as a function of the groove size. The total drag reduction (based on the log-law region comparison), represented by a dashed grey line, as well as the summation of the decomposed terms (□) are included for validation. Minimal channel data is also presented from Modesti *et al.* (2019) (◆).

the Reynolds stress at a y^+ location 3 wall units above the riblet tips. Panels (a)-(d) respectively show the RNL cases with spacings, $s^+ = 10$, 20, 30 and 40, with the $\lambda_z^+ = s^+$ location noted in each figure. The region pertaining to the scales that are relevant to Kelvin-Helmholtz-like rollers ($65 < \lambda_x^+ < 290$ and $250 < \lambda_x^+ < \infty$) are indicated by a box in each panel. Three non-zero streamwise wave numbers spanning $\lambda_x \approx 160, 155,$ and 150 are modeled in the RNL simulations. These modes appear as a single elongated structure in the 2D spectra in figure 3. As expected there is less strong development of the stress in the region associated with the KH rollers for the drag reducing spacings, figures 3(a) and 3(b). However, as the spacing increases, the magnitude of the stress present within the region $65 < \lambda_x^+ < 290$ and $250 < \lambda_x^+ < \infty$ becomes substantial. We also observe that the model accurately predicts the main peak, which is known to be primarily associated with turbulence and the near-wall streaks indicating the model reproduces non-riblet related flow properties. Furthermore, the signature of the dispersive stresses at $\lambda_z^+ = s^+$ for the cases with groove sizes of $\ell_g^+ = 12.65$ and $\ell_g^+ = 18.97$, figures 3(b) and 3(c) are also well modeled by the limited streamwise wave numbers in the RNL dynamics. Finally, we detect the strongest presence of the stresses associated with KH-like rollers for spacings with $\ell_g^+ > 11$, which is consistent with previous observations (García-Mayoral & Jiménez, 2011*b*). It is of note that the normalized magnitude of the RNL spectra is larger than that of the minimal channel due to the fact that energy is constrained to a small number of modes that must contribute to the same total stress observed in the DNS (minimial channel) data that has a full range of streamwise scales. Future work is needed to determine the source of these differences, particularly to extract the Reynolds number differences (in the smooth versus rough wall simulations) and riblet induced physics.

We next quantify the RNL Reynolds stresses that correspond to the spectral region associated with KH-like rollers over blade riblets. We employ a spectral filter based on the added stress from Eqn. (4) using the thresholds outlined in Endrikat *et al.* (2021*a*) to define the profiles as,

$$\overline{u'v'}^{+}_{KH}(y^{+}) = \int_{250}^{\infty}\int_{65}^{290} E^{+}_{uv} \mathrm{d}\lambda^{+}_{x}\lambda^{+}_{y} \tag{7}$$

Here we are integrating over the region denoted in figure 3 at each wall normal position. The profiles obtained by integrating Eqn. (7) for each of the cases in Table 1 are presented in figure 4. Minimal channel data from Endrikat *et al.* (2021*a*) for similar groove spacings are included for a comparison (their precise spacings are noted in the figure). The trends of the RNL modeled stresses show very good agreement to those observed in the minimal channel data, particularly for the drag reducing spacing. For both drag reducing cases there is minimal stress in the region $y^{+} < 20$, which is consistent with the results in figure 2. However even for the $\ell^{+}_{g} = 13$ case, differences arise outside this near-wall region and increase with distance from the wall. Similarly for the drag-increasing riblets, $\ell^{+}_{g} = 19$ and 25, the position of the peak stress above the riblet crest and the magnitude are captured well by the RNL model. However, farther away from the riblets, the RNL model underpredicts the negative stresses compared to the minimal channel results.

CONCLUSIONS

The flow over blade riblets is investigated using a reduced-order model, which severely restricts nonlinearity to that contributing to the streamwise averaged mean (large-scale) dynamics. First and second-order statistics are well captured by the model over the range of riblet spacings considered. The model is then employed to investigate the underlying mechanisms of skin-friction drag changes through a decomposition of the roughness function within the simplified model setting. We focus on the component associated with the added stresses and results indicate that the RNL model generally behaves well for all considered riblet sizes. The drag reducing spacings show very good agreement to known trends while the drag increasing (larger spacings) begin to overpredict the drag present over the riblet geometries, leading to investigations into the added stresses in the drag inducing riblet spacings.

The co-spectra of the Reynolds stress present similar trends to those of full resolution models, including the presence of stresses within the wavenumber ranges associated with Kelvin-Helmholtz-like rollers. The spectra of the reduced order model also capture well the signature of the dispersives stresses at $\lambda^{+}_{z} \approx s^{+}$. Based on the integration of the stress within the region associated with the KH-like instability, we quantify and compare the presence of these rollers as a function of wall-normal location. Again, general trends are well captured by the RNL model, with the magnitude and peak of each profile aligning nicely with those of the minimal channel data. There is again a slight overprediction of these stresses for the RNL model just above the riblet tips, followed by an underprediction of the stress farther from the wall as the sign of the stress changes.

In the future, triangular riblets will be investigated as this geometry is also known to produce Kelvin-Helmholtz structures at drag-increasing spacings (Endrikat *et al.*, 2021*a*). A comparison of the RNL modeled added stresses in the blade and triangular riblets with those in riblet geometries that do not produce KH structures is another direction of ongoing work. Furthermore, we will implement the augmented RNL model introduced in Minnick (2022) which allows non-zero intermediate streamwise modes to interact with small scales. This model led to improved predictions at large Reynolds numbers and we expect it to similarly improve predictions in flow over riblets at larger spacings.

REFERENCES

Bechert, D. W., Bruse, M., Hage, W. V., Van der Hoeven, J. T. & Hoppe, G. 1997 Experiments on drag-reducing surfaces and their optimization with an adjustable geometry. *J. Fluid Mech.* **338**, 59–87.

Bretheim, J. U., Meneveau, C. & Gayme, D. F. 2015 Standard logarithmic mean velocity distribution in a band-limited restricted nonlinear model of turbulent flow in a half-channel. *Phys. Fluids* **27** (1), 011702.

Bushnell, D. 1983 Turbulent drag reduction for external flows. In *21st Aerospace Sciences Meeting*, p. 227.

Chavarin, A. & Luhar, M. 2020 Resolvent analysis for turbulent channel flow with riblets. *AIAA J.* **58** (2), 589–599.

Choi, H., Moin, P. & Kim, J. 1993 Direct numerical simulation of turbulent flow over riblets. *J. Fluid Mech.* **255**, 503–539.

Chung, D., Chan, L., MacDonald, M., Hutchins, N. & Ooi, A. 2015 A fast direct numerical simulation method for characterising hydraulic roughness. *J. Fluid Mech.* **773**, 418–431.

Endrikat, S., Modesti, D., García-Mayoral, R., Hutchins, N. & Chung, D. 2021*a* Influence of riblet shapes on the occurrence of Kelvin–Helmholtz rollers. *J. Fluid Mech.* **913**.

Endrikat, S, Modesti, D, MacDonald, M, García-Mayoral, R, Hutchins, N & Chung, D 2021*b* Direct numerical simulations of turbulent flow over various riblet shapes in minimal-span channels. *Flow, Turbulence and Combustion* **107** (1), 1–29.

Farrell, Brian F & Ioannou, Petros J 2012 Dynamics of streamwise rolls and streaks in turbulent wall-bounded shear flow. *J. Fluid Mech.* **708**, 149–196.

García-Mayoral, R. & Jiménez, J. 2011*a* Drag reduction by riblets. *Philos. Trans. R. Soc. London, Ser. A* **369** (1940), 1412–1427.

García-Mayoral, R. & Jiménez, J. 2011*b* Hydrodynamic stability and breakdown of the viscous regime over riblets. *J. Fluid Mech.* **678**, 317.

Garcia-Mayoral, R., Gómez-de Segura, G. & Fairhall, C. T. 2019 The control of near-wall turbulence through surface texturing. *Fluid Dyn. Res.* **51** (1), 011410.

Gayme, D. F. & Minnick, B. A. 2019 Coherent structure-based approach to modeling wall turbulence. *Phys. Rev. Fluids* **4** (11), 110505.

Goldstein, D. B. & Tuan, T. C. 1998 Secondary flow induced by riblets. *J. Fluid Mech.* **363**, 115–151.

Jelly, T. O., Jung, S. Y. & Zaki, T. A. 2014 Turbulence and skin friction modification in channel flow with streamwise-aligned superhydrophobic surface texture. *Phys. Fluids* **26** (9), 095102.

JHU-LESGO 2019 Lesgo: A parallel pseudo-spectral large-eddy simulation code. `https://lesgo.me.jhu.edu`.

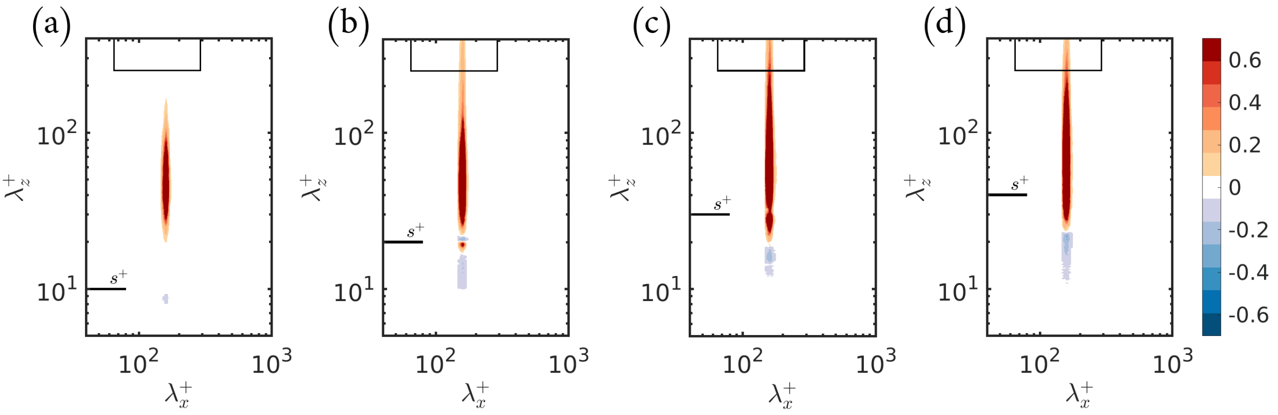

Figure 3. Premultiplied co-spectra of the Reynolds stress, $k_x^+ k_z^+ E_{uv}^+$, of the drag reducing riblet spacings (a) $\ell_g^+ = 6.33$ and (b) $\ell_g^+ = 12.65$ as well as the drag increasing spacings (c) $\ell_g^+ = 18.97$ and (d) $\ell_g^+ = 25.30$. The spectra are taken at a plane located 3 wall units above the riblet tips, $y^+ = \ell_T^+ + 3$, and normalized by $\overline{u'v'}^+$.

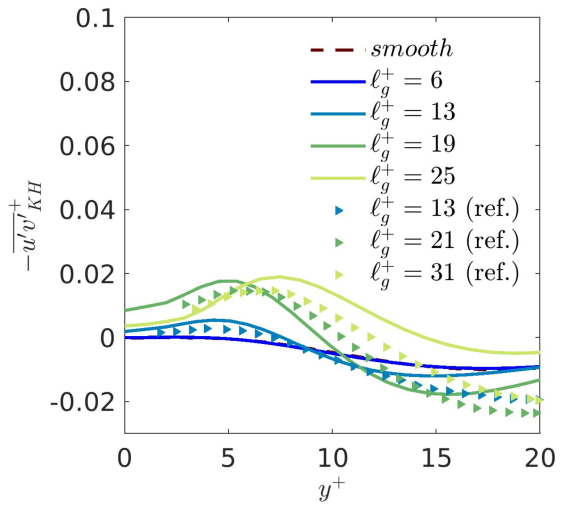

Figure 4. Stress contributions due to Kelvin-Helmholtz-like rollers based on the integration of the Reynolds stress 2D co-spectra in Eqn. (7) of the RNL model are given as a function of wall-normal location. Data for similar groove spacings are also included from Endrikat *et al.* (2021*a*) (minimal channel).

Jiménez, J. 2004 Turbulent flows over rough walls. *Annu. Rev. Fluid Mech.* **36**, 173–196.

Luchini, P. 1996 Reducing the turbulent skin friction. In *Computational methods in applied sciences '96 (Paris, 9-13 September 1996)* (ed. J. A. Désidéri, C. Hirsch, P. Le Tallec, E. Oñate, M. Pandolfi, J. Périaux & E. Stein), pp. 465–470. John Wiley, Chichester United Kingdom.

Luchini, P., Manzo, F. & Pozzi, A. 1991 Resistance of a grooved surface to parallel flow and cross-flow. *J. Fluid Mech.* **228**, 87–109.

Minnick, B. A. 2022 A restricted nonlinear approach to momentum and scalar mixing in wall-turbulence. PhD thesis, Johns Hopkins University.

Minnick, B. A. & Gayme, D. F. 2019 Characterizing energy transfer in restricted nonlinear wall-bounded turbulence. In *Proc. of 11th International Symposium on Turbulence and Shear Flow Phenomena*.

Modesti, D., Endrikat, S., García-Mayoral, R., Hutchins, N. & Chung, D. 2019 Contribution of dispersive stress to skin friction drag in turbulent flow over riblets. In *Proc. of 11th International Symposium on Turbulence and Shear Flow Phenomena*.

Modesti, Davide, Endrikat, Sebastian, Hutchins, Nicholas & Chung, Daniel 2021 Dispersive stresses in turbulent flow over riblets. *J. Fluid Mech.* **917**.

Peskin, Charles S 2002 The immersed boundary method. *Acta numerica* **11**, 479–517.

Spalart, P. R. & McLean, J. D. 2011 Drag reduction: enticing turbulence, and then an industry. *Phil. Trans. R. Soc. A* **369** (1940), 1556–1569.

Thomas, V., Farrell, B., Ioannou, P. & Gayme, D. F 2015 A minimal model of self-sustaining turbulence. *Phys. Fluids* **27**, 105104.

Thomas, V. L., Lieu, B. K., Jovanović, M. R., Farrell, B. F., Ioannou, P. J. & Gayme, D. F. 2014 Self-sustaining turbulence in a restricted nonlinear model of plane couette flow. *Phys. Fluids* **26** (10), 105112.

Vinokur, M. 1983 On one-dimensional stretching functions for finite-difference calculations. *J. Computational Phys.* **50** (2), 215–234.

Viswanath, P. R. 2002 Aircraft viscous drag reduction using riblets. *Prog. Aerosp. Sci.* **38** (6-7), 571–600.

Walsh, M. 1980 Drag characteristics of V-groove and transverse curvature riblets. In *Symp. on Viscous Flow Drag Reduction*.

Walsh, M. 1982 Turbulent boundary layer drag reduction using riblets. In *Proc. the 20th Aerospace Sciences Meeting*, p. 169.